Journal of the Iranian Chemical Society (2019) 16:1735–1748
https://doi.org/10.1007/s13738-019-01647-w

ORIGINAL PAPER

Comparison of MIL-101(Fe) and amine-functionalized MIL-101(Fe) as photocatalysts for the removal of imidacloprid in aqueous solution

Cihan Gecgel[1,2] · Utku Bulut Simsek[1] · Belgin Gozmen[1,3] · Meral Turabik[1,4]

Received: 5 November 2018 / Accepted: 22 February 2019 / Published online: 26 February 2019

Abstract

One of the attractive iron-based metal organic framework (MOF) MIL-101(Fe) (Material Institute Lavoisier, MIL) and amine-functionalized NH_2-MIL-101(Fe) materials were synthesized by conventional solvothermal method and characterized by TGA (Thermo Gravimetric Analysis), SEM (Scanning Electron Microscopy), XRD (X-Ray Diffractograms), BET (Braunner Emmet Teller) and FTIR (Fourier Transform Infrared Spectroscopy). Characterization results indicated that MIL-101(Fe) materials have well defined morphology, good thermal stability, high surface area and also high porosity. These MOF materials were used as photocatalysts for photodegradation of a pesticide, imidacloprid (IMC). The response surface methodology (RSM) was applied in designing the IMC photodegradation experiments for evaluating the interactive effects of independent variables and determining the optimum condition. Central composite design as five independent variables such as initial MIL-101(Fe) concentration, initial IMC concentration, H_2O_2 concentration, pH and time were coded with low and high level and IMC removal percent was obtained as a response. As for the RSM results on the optimum photocatalytic condition, maximum IMC removal values were determined as 100% for the both catalysts in the end of the 30 min. The adsorption efficiencies of catalysts were also investigated and obtained results showed that amine-functionalized MIL-101(Fe) was the more effective sorbent than MIL-101(Fe).

Keywords Metal organic frameworks (MOFs) · MIL-101(Fe) · Amine functionalization · Photocatalyst · Adsorption · Response surface methodology (RSM)

Introduction

Metal organic frameworks (MOFs) are a class of porous coordination polymers consisting of metal-containing nodes and organic binders. Most of MOFs have superior features such as tunable pore sizes, large specific surface areas, high temperature stability, reactivity/photocatalytic reactivity and adsorption abilities. Due to these important features, MOFs have been used in different application areas such as catalysis, gas storage/capture, purification, chemical and luminescence sensors, drug delivery, and separation [1–6]. One of the MOFs, Al^{3+}, Fe^{3+}, and Cr^{3+}, based MILs (Materials of Institut Lavoisier) series, have been of great interest due to their high stability and available raw materials [7, 8]. Iron-based MILs have specific textural properties such as wide distribution of single iron sites, porous structures and large surface areas which give the advantages in different application areas [9].

However, the use of most MOFs, especially in catalysis or separation process, is still largely limited by the lack of functional and selective sites in its frameworks [10]. It is possible to increase the efficiency of MOFs by functioning and modifying [9, 11]. Functional MOFs have been provided either direct synthesis of materials using ligand containing functional group (pre-functionalized procedure) or post-synthetic modification of parent materials (PSM) [9, 11]. But, most of the studies existing in the literature have showed that post-synthetic functionalized MOFs are a limited stability [9]. Thus, much interest has been recently

✉ Meral Turabik
mturabik@mersin.edu.tr

1 Department of Nanotechnology and Advanced Materials, Mersin University, Mersin, Turkey

2 Advanced Technology Education Research and Application Center, Mersin University, Mersin, Turkey

3 Department of Chemistry, Faculty of Science and Letters, Mersin University, Mersin, Turkey

4 Chemical Program, Technical Science Vocational School, Mersin University, Mersin, Turkey

devoted on pre-functionalized MOFs which obtained by incorporation of ligands including additional functional groups (–NH_2, –OH, SO_3…) with metal-containing nodes. Functional groups are attached into the phenyl rings of the organic backbones by hydrothermal/solvothermal reactions [10, 12–17]. Especially amine-functionalized MOFs (NH_2-MOF) have mainly attracted attention because of their basic amine sites, which have a strong affinity for acidic gas molecules and active sites for catalysis [13]. Amine-functionalized MOFs can lead to the binding of analyte molecules through hydrogen bonding and induce electron transfer between MOFs and analytes [14].

Pesticides are widely used to manage weeds, insects and disease infestation [15]. In the recent years, various pesticides have been frequently detected in natural water source, soil and also air environments because of widespread use in many areas [11, 16]. People can get serious diseases (cancer, chronic obstructive pulmonary disease, birth defects, infertility) when they come into contact with pesticide residues [16]. In recent years, one of the neonicotinoid pesticides, imidacloprid (IMC) have been used extensively for protecting crops from insect pests. It is the bestselling and most preferred neonicotinoid pesticides on the world due to a higher lethal effect for insects, but it can be hazardous for non-target organisms and threated to human life [17, 18]. IMC can be available for a long time in ecosystems via spray drift, surface runoff and ground water leaching, and also can seriously contaminates ecosystems because of its high solubility in water (0.58 g/L) and remains stable in it approximately between 30 and 50 days [19, 20]. Consequently, it is crucial to develop effective treatment methods to remove the undesirable pesticide residues in environment. For this purpose, among various physical, chemical and biological methods, especially adsorption and advanced oxidation processes (AOPs) are increasingly adopted to the removal/destruction of organic contaminants, because of their high efficiency, simplicity, good reproducibility, and easy handling [21].

Recent studies have shown that metal organic frameworks (MOFs) have a huge potential and bright perspective in photocatalytic degradation and adsorptive removal of different organic pollutants [2]. MOFs are promising photocatalysts due to their semiconductor-like behavior under irradiation. The photo-excitation of MOFs will cause form electrons (e^-) and holes (h^+) in the structure. The metal sites of MOF structure can be activated by transition from ligand to metal cluster [22, 23].

In the present study, one of the iron-based metal–organic framework MIL-101(Fe) and its amine-functionalized form, NH_2-MIL-101(Fe), were synthesized by means of conventional solvothermal method. These MILs (Fe) materials were used as catalysts for the removal of IMC by a combined process of adsorption and photocatalytic degradation. To the best our knowledge, a few reports exist on the removal of pesticides by the combined processes with metal organic frameworks. The effects of independent variables considered to be effective in the photocatalytic oxidation of IMC were investigated using the response surface method (RSM). RSM is a chemometric technique involving various statistical design methods. By using RSM, the effects of the independent variables on the response are examined with minimize the consumption of time, reagents and workload, and the appropriate optimum conditions are determined [24, 25]. The experiments were designed according to central composite design (CCD) to determine the influence of factors, such as catalyst amounts, initial IMC concentration, H_2O_2 concentrations, pH and time on the degradation as well as studying the optimum working state.

Materials and methods

Chemicals

For the synthesis of MIL-101(Fe) materials, iron chloride hexahydrate ($FeCl_3{\cdot}6H_2O$), terephthalic acid (H_2BDC), 2-aminoterephthalic acid (NH_2–H_2BDC), dimethylformamide (DMF) and ethanol were purchased from Sigma-Aldrich Dresden Germany. Imidacloprid ($C_9H_{10}ClN_5O_2$) was also purchased Sigma-Aldrich Dresden Germany and its chemical formula is given in Fig. 1.

Preparation of MOF materials

MIL-101 (Fe) was synthesized and developed according to literature report [26]. In brief, 2.48 mmol $FeCl_3{\cdot}6H_2O$ and 1.24 mmol H_2BDC were added to 20 mL DMF and mixture was stirred by magnetic stirrer. Then the homogenous dissolved solution was heated 110 °C for 20 h in a Teflon reactor. Then the first product was centrifuged at 13.000 rpm

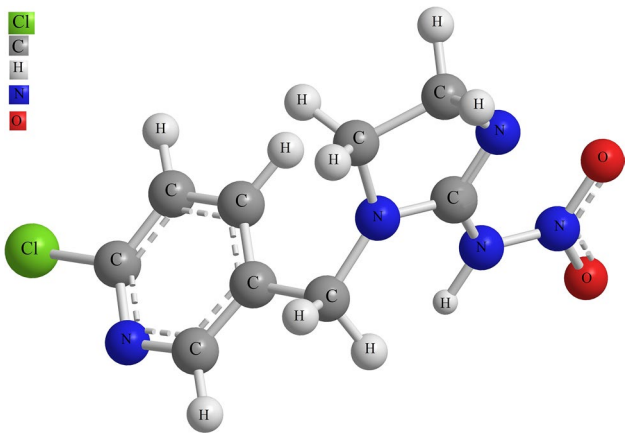

Fig. 1 Chemical formula of IMC

and purified by washing hot DMF (70 °C, 15 min) several times (Fig. 2). The purified light orange product was dried in a vacuum oven at 70 °C overnight. For the amine-functionalized MIL-101(Fe) synthesis, NH_2-MIL-101(Fe), the 1.24 mmol 2-aminoterephthalic acid (NH_2–H_2BDC) was used instead of H_2BDC and followed by the same synthesis procedure [26] and product were obtained as dark brown color (Fig. 2).

Analyses of MOF materials

The Scanning Electron Microscopy (SEM) images and Energy Dispersive X-ray (EDX) chemical analysis of MIL-101(Fe) materials were recorded with a Zeiss Supra 55 field emission SEM. Samples were coated under vacuum with platinum/palladium prior to the analysis to increase the surface conductivity. X-ray diffractograms (XRD) of MIL-101(Fe) samples were performed using a Rigaku Smartlab model XRD at Cu-Kα radiation ($\lambda = 1.54$ Å). The analysis of dried MIL-101(Fe) materials were carried out in continuous scans from 2° to 20° at 2 scan rate at 2 theta min^{-1} in ambient air. The FTIR measurements were also performed with Perkin Elmer/MIR spectrometer and a Pike Technologies Gladi ATR accessory. The FTIR spectra were obtained with the MIR mode at a constant ambient temperature of 25 °C by accumulating 10 scans at a 1 cm^{-1} resolution in the 4000–450 cm^{-1} region. Nitrogen adsorption isotherms were measured − 196 °C using a Micromeritics Tristar Orion II 3020 surface area and porosimetry analyzer. According to the resulting isotherms of the MIL-101(Fe) samples, Brunauer–Emmett–Teller (BET) method was used for the analysis of surface area. Thermogravimetric analysis (TGA) was performed on a Mettler Toledo TGA/DSC 3 + thermogravimetric analyzer from room temperature to 600 °C at a ramp rate 10 °C/min.

The photocatalytic oxidation experiments

The photocatalytic activities of MIL-101(Fe) and NH_2-MIL-101(Fe) catalysts were performed by the photodegradation of IMC with H_2O_2 oxidant under 150 W Blue LED light source (Kessil, > 400 nm) irradiation in open air and at room temperature. The distance between the solution and the light source was set to 15 cm and the solution was mixed with the magnetic stirrer. Each catalyst was added to 35 mL of the IMC solution and pH of the solution was adjusted to the desired value using H_2SO_4 and NaOH solutions. While the light source was turned off, the mixture of IMC solution and catalyst were stirred for 1 h to ensure the adsorption—desorption equilibrium. Samples were taken to calculate the amount of adsorption. For further photocatalytic treatment, the light was then turned on and H_2O_2 was added in the determined amount. Quantitative analysis of imidacloprid was detected using an Agilent 1200 Series high pressure liquid chromatography (HPLC) system equipped with an ACE C_{18} Column (10 × 250 mm particle size 5 µm) using a mobile phase composed of water/acetonitrile (70:30, v/v) at a flow rate of 1 mL/min, the column temperature was 30 °C Diode Array Detector (DAD) was operated with 270 nm. Reusability of MIL-101(Fe) materials was examined in four cycles. In the reusability experiment, the

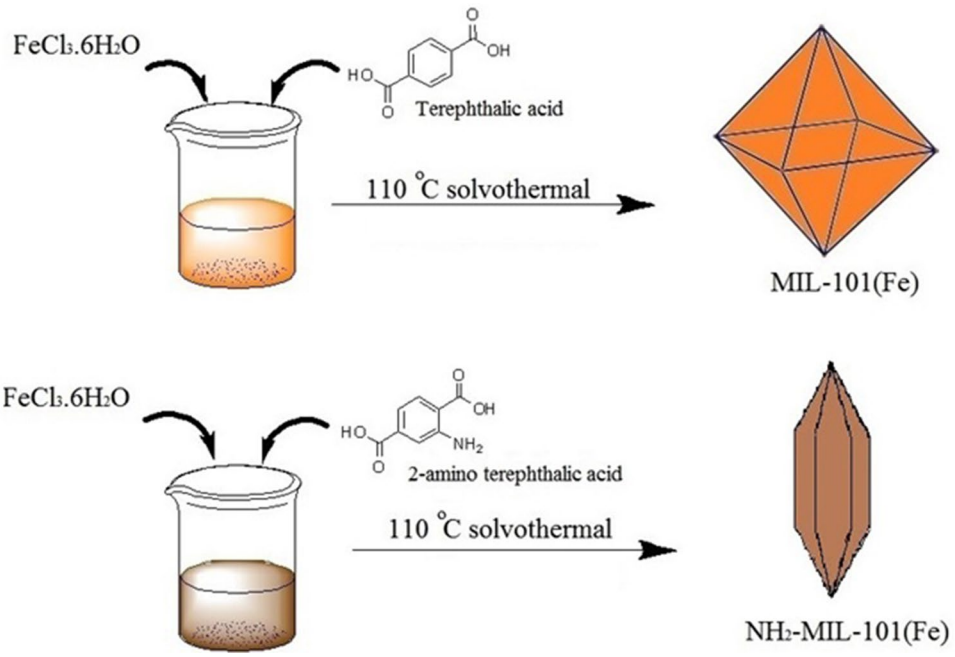

Fig. 2 The synthesis schema of MIL-101(Fe) MOF materials

Table 1 The levels and codes of the factors in the CCD (central composite design)

Factors	Levels and codes				
	−α	−1	0	+1	+α
X_1:Cat (g/L)	0.06	0.12	0.16	0.20	0.26
X_2:IMC (mg/L)	12	40	60	80	108
X_3:H_2O_2 (μL)	23	75	113	150	202
X_4:pH	3.0	5.0	6.5	8.0	10.0
X_5:time (min)	5	15	23	30	40

Table 2 Basic characteristics of the catalysts

	Morphology	BET surface area m^2/g	Pore size Å	Color
MIL-101 (Fe)	Octahedral	2865	9.02	Light orange
NH_2-MIL-101(Fe)	Microspindle	1137	8.84	Dark brown

MIL-101-(Fe) materials were separated using centrifuge and washed thoroughly with deionized water and ethanol.

Experimental design and optimization

The effects of five independent variables on photocatalytic degradation of IMC solution were studied by central composite design (CCD) at five levels. The names, levels and codes of these variables are given in Table 1. In this design, depending on the factor of k, the number of experiments (*N*) was calculated by the following formula:

$$N = 2^k + 2k + 8 \quad (1)$$

N was determined as 50 in this study and the central composite experimental design results are given in Table 2.

Results and discussion

Characterization of MOF materials

The MIL-101(Fe) materials were characterized by SEM /EDX, XRD, TGA, FTIR, and BET surface area analyzer. SEM images and EDX results of MIL-101(Fe) and NH_2-MIL-101(Fe) are given in Fig. 3. The SEM image in Fig. 3a, revealed that all of the MIL-101(Fe) particles were uniform octahedral morphology. As shown in Fig. 3b, the synthesized NH_2-MIL-101(Fe) has a hexagonal microspindle morphology with uniform particle distribution. The composition and distribution analysis by EDX measurement of the MIL-101(Fe) samples are also illustrated in Fig. 3a. In resulting values from platinum and palladium coating were neglected and the percent of Fe, O, C, N, Cl elements were obtained as 38.37, 30.12, 22.20, 0.00, 9.31% for MIL-101(Fe) and 30.94, 22.83, 36.17, 3.73, 6.33% for NH_2-MIL-101(Fe), respectively. The presence of the nitrogen content in NH_2-MIL-101(Fe) proves that the amination process took place.

The XRD patterns of MIL-101(Fe) and NH_2-MIL-101(Fe) samples are illustrated in Fig. 4a, b, respectively. As given in literature, Fig. 4a indicates that the typical characterization peaks of MIL-101(Fe) can be seen at 4.84°, 9.42°, 9.66° and 18.88° at fairly high intensity [27, 28]. On the other hand, NH_2-MIL-101(Fe) has similar two diffraction peaks to MIL-101(Fe) and these peaks are observed at 9.38° and 18.88° at 2 theta degrees [27–30]. As a conclusion the XRD patterns suggest that MIL-101(Fe) and NH_2-MIL-101(Fe) have a higher degree of crystallinity.

Fig. 5 the TGA results in Fig. 5 shows that the weight losses of MIL-101(Fe) and NH_2-MIL-101(Fe) occur in three steps. In the first step, due to the evaporation of water or solvent molecules present inside the pore and surface of the frameworks, weight loss has occurred as 7.91% for MIL-101(Fe) and 7.93% for NH_2-MIL-101(Fe) in the range of 50–150 °C temperature. The first step is inevitable for MIL-101(Fe) materials with high moisture holding capacity. In the first step, MIL-101(Fe) and NH_2-MIL-101(Fe) have showed a similar tendency in the TGA curve. In the second step, weight losses observed at a temperature range of 150–340 °C as 18.27% for MIL-101(Fe) and 10.36% for NH_2-MIL101(Fe) may be due to the elimination of OH, Cl, and NH_2 groups [26]. The less weight loss observed for NH_2-MIL-101(Fe) also suggests that it is thermally more stable than MIL-101(Fe). In the third step, weight losses observed both MIL-101(Fe) and NH_2-MIL-101(Fe) structures at over the 440 °C temperatures were due to decomposition of the TPA. At the end of the third step, the total weight losses of the MIL-101(Fe) and NH_2-MIL-101(Fe) were 40.51% and 36.10%, respectively.

The FTIR of MIL-101(Fe) and NH_2-MIL-101(Fe) are given in Fig. 6. The peaks derived from terephthalic acid were obtained from asymmetric and symmetrical C–O bonds at 1661, 1595 and 1653, 1579 cm^{-1}, respectively. In addition, the apparent peaks at 552 cm^{-1} for MIL-101(Fe) and 521 cm^{-1} for NH_2-MIL-101(Fe) are related to the Fe–O vibration. It was seen that all characteristic peaks of the MIL-101(Fe) spectrum shifted slightly to the left for the NH_2-MIL-101(Fe) spectrum. In Fig. 6, NH_2-MIL-101(Fe) has also two asymmetric and symmetric N–H stretches of low intensity at 3300 and 3500 cm^{-1} in the FTIR spectrum. In addition, the peak observing at 1257 cm^{-1} in the NH_2-MIL-101(Fe) can be said to be a characteristic peak of C–N bonds originating from aromatic amine groups. Similar

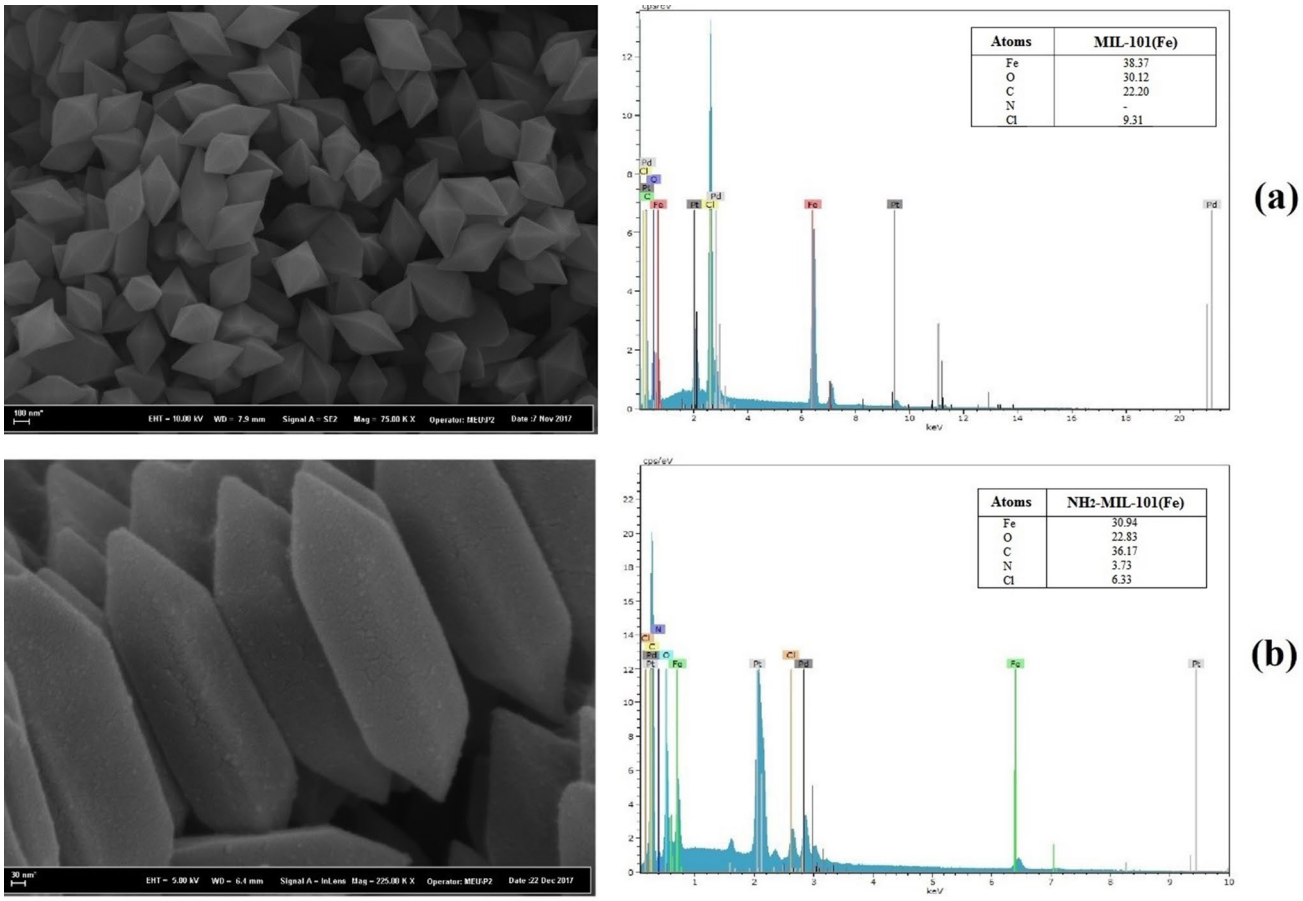

Fig. 3 SEM Images of MIL-101 MOF materials **a** MIL-101(Fe), **b** NH_2-MIL-101(Fe)

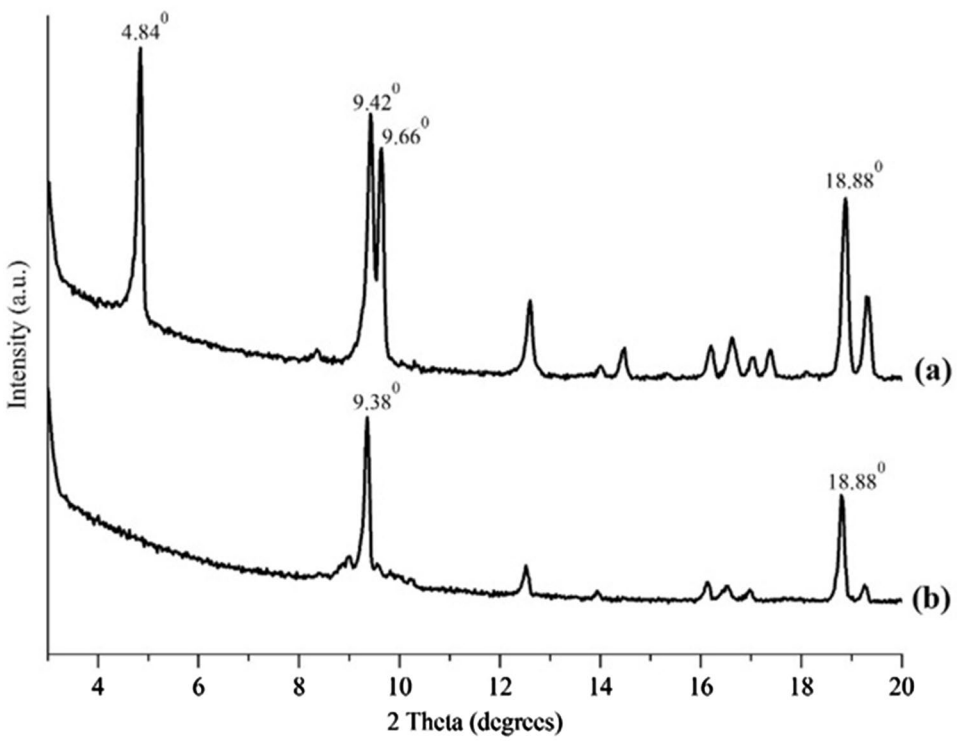

Fig. 4 XRD patterns of MIL-101 MOF materials **a** MIL-101(Fe), **b** NH_2-MIL-101(Fe)

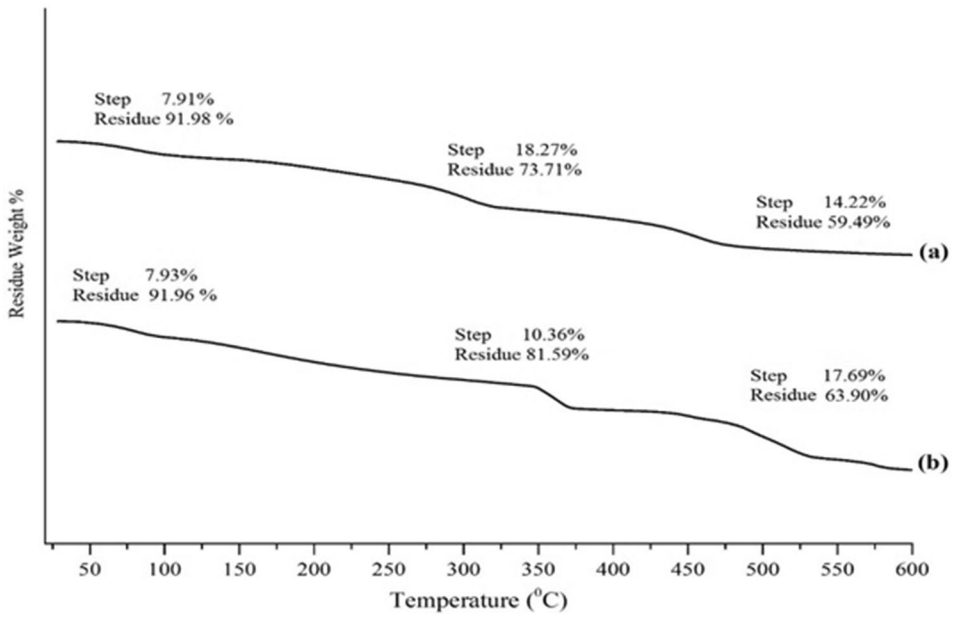

Fig. 5 TGA curve of MIL-101 MOF materials **a** MIL-101(Fe), **b** NH_2-MIL-101(Fe)

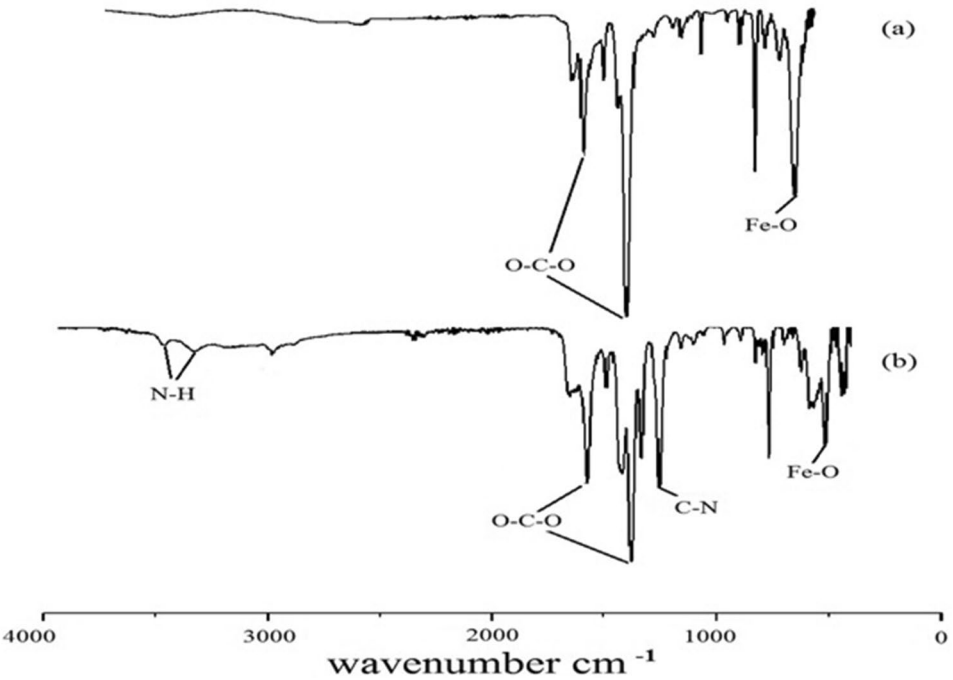

Fig. 6 FTIR Spectra of MIL-101 MOF materials **a** MIL-101(Fe), **b** NH_2-MIL-101(Fe)

FTIR peaks for the MIL-101(Fe) and NH_2-MIL-101(Fe) have been reported in the literature [26, 30–32].

Nitrogen adsorption isotherms of MIL-101(Fe) and NH_2-MIL-101(Fe) are presented in Fig. 7. Figure 7 indicates that the MIL-101(Fe) and NH_2-MIL-101(Fe) nitrogen adsorption isotherms were compatible with type I isotherm. This isotherm is characteristic isotherm of microporous materials [33]. According to this knowledge MIL-101(Fe) and NH_2-MIL-101(Fe) are microporous materials. Porosity and surface properties of MIL-101(Fe) materials were calculated Barret-Joyner-Halenda (BJH) equation [34] and Braunner–Emmett–Teller (BET) equation [35], respectively. BET surface area of the MIL-101(Fe) and NH_2-MIL-101(Fe) were determined from the adsorption isotherms as 2865 m^2/g and 1137 m^2/g, respectively. The pore diameter of MIL-101(Fe) and NH_2-MIL-101(Fe) were also measured as 9.02 Å and 8.84 Å, respectively. These results showed that BET surface area and porosity decreased by the amination of MIL-101(Fe). By the amine functionalization, the amine molecules are directed towards the center of the microporous cages, which makes nitrogen diffusion difficult as well as causes partial occupation of the space

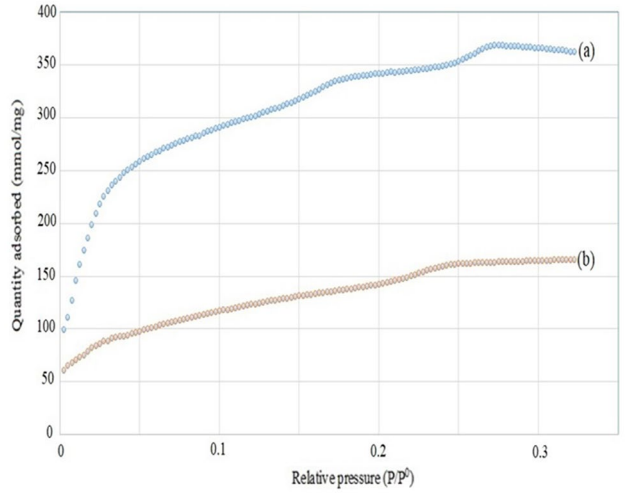

Fig. 7 BET isotherm plot of MIL-101 MOF materials **a** MIL-101(Fe), **b** NH_2-MIL-101(Fe)

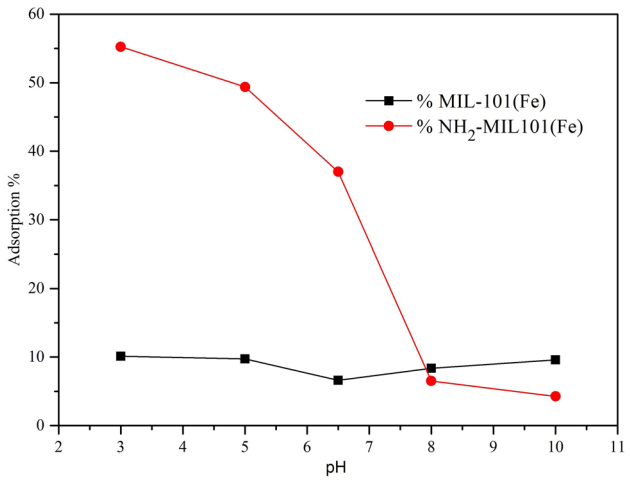

Fig. 8 The effect of pH on the adsorption % of the catalysts (IMC = 60 mg/L, Catalyst = 0.20 g/L)

inside the pores. Along with that a slight decrease in pore size and also surface area can be expected [33]. After the characterization of the materials, results were evaluated and basic properties of the MIL-101(Fe) and NH_2-MIL-101(Fe) materials are summarized in Table 2. As seen in Table 2, the structure of MIL-101(Fe) changed significantly after amine functionalization.

Adsorption of imidacloprid

Before the photocatalytic degradation process, adsorption of IMC by the catalysts was investigated at different pH values for 1 h and given in Fig. 8. When the pH value of IMC solution increased from 3 to 10, the removal values of IMC by adsorption on NH_2-MIL-101(Fe) decreased to 55.3–4.3%, respectively. For the MIL-101(Fe), while the adsorption values of IMC were about 10% both at acidic and basic pH values, the adsorption value decreased to 7% at about neutral pH (pH 6.5) (Fig. 8). The results showed that the adsorption power of the NH_2-MIL-101(Fe) catalyst was significantly higher than that of MIL-101(Fe) and also found to be much more effective at acidic pH values.

Pore structure, electrostatic interaction, π-π interaction, hydrogen bonding and acid-base interactions may affect adsorption efficiency of MOFs in aqueous solutions [36, 37]. The higher adsorption with NH_2-MIL-101(Fe), which has a lower surface area and porosity than MIL-101(Fe), is due to predominant hydrogen bonding effect. On the other hand, IMC possess two pKa values (i.e., 1.56 and 11.12) in which the major species of IMC were cationic (IMC^+) at pH < 1.56, and anionic (IMC^-) at pH > 11.12 [38]. It is known that the amino group from NH_2-MIL-101(Fe) acts as a Lewis base [39], in this case it may electrostatic interact with IMC^+ at acidic pH values.

When the effect of catalyst amount on adsorption was also examined, the removal values of 40 mg/L of IMC solution at pH 5 using 0.12 g/L and 0.20 g/L of NH_2-MIL-101(Fe) were obtained as 54.9% and 67.9%, respectively. When the same study was carried out at pH 8, the percentage of removal increased only from 4.11 to 4.51%. So, these results showed that the catalysts amounts are effective parameter for the adsorption of IMC.

Evaluation of the obtained model by ANOVA

The removal of IMC was carried out by the photocatalytic experiments by using MIL-101(Fe) and NH_2-MIL-101(Fe) as catalysts and the results were given in Tables 2 and 3. For both catalysts, the model fitted was observed to be 2FI (2-factor interactions.) The quality of the model fitted was evaluated by analysis of variance (ANOVA). When the results of ANOVA of the models were examined for both catalysts (Tables 3, 4), it was observed that the F values of MIL-101(Fe) and NH_2-MIL-101(Fe) catalysts were higher than the tabulated F value $\left[F_{0.05,df(n-(df+1))}\right]$ with a very low p values (< 0.0001). A small p value (Prob > F) indicated that the interaction terms have improved the model. For this reason, terms with a large p value were excluded. For MIL-101(Fe) and NH_2-MIL-101(Fe) catalysts, another indicator of the model fit, R^2 (R^2adj) values were found as 0.9150 (0.8932) and 0.9201 (0.9021), respectively.

Multiple regression modeling

The obtained model fitted equations for photocatalytic removal of IMC with MIL-101(Fe) and NH_2-MIL-101(Fe) catalysts were shown below:

Table 3 Central composite experimental design and results of photocatalytic degradation of IMC

Run	Factors					Removal %	
	x_1	x_2	x_3	x_4	x_5	MIL-101(Fe)	NH_2-MIL-101(Fe)
1	0.12	40	75	5.0	15	43.5	56.0
2	0.20	40	75	5.0	15	53.8	65.7
3	0.12	80	75	5.0	15	49.2	31.4
4	0.20	80	75	5.0	15	40.1	52.7
5	0.12	40	150	5.0	15	75.1	43.4
6	0.20	40	150	5.0	15	83.6	73.1
7	0.12	80	150	5.0	15	29.2	40.3
8	0.20	80	150	5.0	15	41.3	50.0
9	0.12	40	75	8.0	15	12.4	5.5
10	0.20	40	75	8.0	15	10.0	8.1
11	0.12	80	75	8.0	15	11.5	5.7
12	0.20	80	75	8.0	15	8.6	5.8
13	0.12	40	150	8.0	15	13.9	8.6
14	0.20	40	150	8.0	15	22.3	9.2
15	0.12	80	150	8.0	15	9.5	5.2
16	0.20	80	150	8.0	15	7.4	6.1
17	0.12	40	75	5.0	30	70.2	64.0
18	0.20	40	75	5.0	30	92.9	94.4
19	0.12	80	75	5.0	30	100	51.4
20	0.20	80	75	5.0	30	87.6	92.2
21	0.12	40	150	5.0	30	92.9	87.3
22	0.20	40	150	5.0	30	100	83.6
23	0.12	80	150	5.0	30	83.2	97.4
24	0.20	80	150	5.0	30	84.9	77.7
25	0.12	40	75	8.0	30	12.4	5.8
26	0.20	40	75	8.0	30	10.6	8.4
27	0.12	80	75	8.0	30	13.6	9.2
28	0.20	80	75	8.0	30	11.6	6.1
29	0.12	40	150	8.0	30	16.4	10.7
30	0.20	40	150	8.0	30	19.8	12.3
31	0.12	80	150	8.0	30	11.8	6.2
32	0.20	80	150	8.0	30	14.1	6.2
33	0.06	60	113	6.5	23	30.2	11.4
34	0.26	60	113	6.5	23	69.6	71.3
35	0.16	12	113	6.5	23	87.8	50.0
36	0.16	108	113	6.5	23	14.5	31.8
37	0.16	60	23	6.5	23	23.6	29.1
38	0.16	60	202	6.5	23	57.1	53.3
39	0.16	60	113	3.0	23	100	100
40	0.16	60	113	10	23	0.6	0.4
41	0.16	60	113	6.5	5	12.3	36.6
42	0.16	60	113	6.5	40	66.4	77.0
43	0.16	60	113	6.5	23	50.3	40.2
44	0.16	60	113	6.5	23	51.2	39.9
45	0.16	60	113	6.5	23	53.6	37.3
46	0.16	60	113	6.5	23	51.6	43.2
47	0.16	60	113	6.5	23	50.7	42.7
48	0.16	60	113	6.5	23	58.8	36.5

Table 3 (continued)

Run	Factors					Removal %	
	x_1	x_2	x_3	x_4	x_5	MIL-101(Fe)	NH_2-MIL-101(Fe)
49	0.16	60	113	6.5	23	58.1	44.4
50	0.16	60	113	6.5	23	54.7	37.9

Table 4 ANOVA results of modified 2FI models for the catalysts obtained by CCD

Source	MIL-101(Fe)				NH_2-MIL-101(Fe)			
	Sum of squares	*df*	*F* value	*p* value Prob > *F*	Sum of squares	*df*	*F* value	*p* value Prob > *F*
Model	41,811	10	42.00	< 0.0001	38,288	9	51.17	< 0.0001
X_1:Cat	436	1	4.37	0.0426	1902	1	22.88	< 0.0001
X_2:IMC	1478	1	14.85	0.0004	553	1	6.65	0.0137
X_3:H_2O_2	571	1	5.73	0.0216	202	1	2.43	0.1271
X_4:pH	30,953	1	310.92	< 0.0001	31,032	1	373.27	< 0.0001
X_5:time	4452	1	44.72	< 0.0001	2412	1	29.01	< 0.0001
X_1 X_2	147	1	1.48	0.2316	–	–	–	–
X_1 X_3	–	–	–	–	129	1	1.55	0.2201
X_1 X_4	–	–	–	–	560	1	6.74	0.0132
X_2 X_3	791	1	7.95	0.0075	–	–	–	–
X_2 X_4	139	1	1.40	0.2440	177	1	2.13	0.1519
X_2 X_5	374	1	3.76	0.0597	–	–		
X_4 X_5	2469	1	24.81	< 0.0001	1322	1	15.90	0.0003
Residual	3882	39			3639	40		
Lack of fit	3805	32	10.73	0.0016	3578	33	11.48	0.0013
Pure error	77.55	7			60.34	7		
Cor total	45,693	49			44,003	49		

$$\text{Removal\% (MIL-101(Fe))} = +44.09 + 3.17x_1 - 5.84x_2 + 3.63x_3 - 26.73x_4 + 10.14x_5 - 2.14x_1x_2 - 4.97x_2x_3 + 2.09x_2x_4 + 3.42x_2x_5 - 8.78x_4x_5 \quad (2)$$

$$\text{Removal\% (NH_2-MIL-101(Fe))} = +39.47 + 5.93x_1 - 4.27x_2 + 1.47x_3 - 27.46x_4 + 8.15x_5 - 3.25x_1x_4 + 3.29x_2x_4 - 7.37x_4x_5 \quad (3)$$

In both equations, when the effects of the independent variables on the responses are examined, it is seen that the effects of the x_1, x_3 and x_5 parameters are positive and the x_2 and x_4 parameters are effective in the negative direction. The most effective variable is x_4 (pH), and the increase of this variable causes to decrease in removal% of IMC. The second effective variable, x_5 (time), leads to an increase in removal % of IMC.

Photocatalytic degradation of imidacloprid

The effect of catalyst/UV/H_2O_2 system

Photocatalytic efficiencies of catalysts on IMC removal were examined for alone catalyst, together with UV (catalyst/UV) and H_2O_2 (catalyst/H_2O_2) and also catalyst/UV/H_2O_2 system without pH adjustment and given in Fig. 9. After the catalysts addition to IMC solution, the solutions

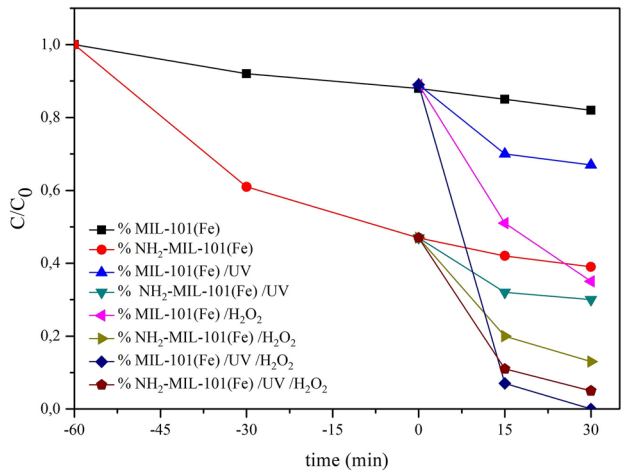

Fig. 9 The effects of catalysts on IMC degradation in different applications (IMC = 40 mg/L, Catalyst = 0.16 g/L, H_2O_2 = 150 µL)

pH values were measured as 3.74 and 4.17 for MIL-101(Fe) and NH_2-MIL-101(Fe), respectively.

When Fig. 9 was examined, the catalyst was alone in solution, it was observed that after 1-h adsorption–desorption equilibrium, the adsorption of the IMC continued as a low level for the next 30 min for both catalysts. While the combined use of MIL-101(Fe)/UV or NH_2-MIL-101(Fe)/UV was applied to photodegradation, it was determined that catalysts/UV systems were not very effective on IMC removal. However, the combined catalysts/H_2O_2 systems (MIL-101(Fe)/H_2O_2 or NH_2-MIL-101(Fe)/H_2O_2) were more effective than catalysts/UV systems. Figure 9 shows also that the catalyst/UV/H_2O_2 systems were the best effective systems for the photocatalytic removal of IMC for both catalysts.

For the combined catalyst/UV/H_2O_2 system, however, it was determined that MIL-101(Fe) was the more effective photocatalyst than NH_2-MIL-101(Fe). These results showed that the NH_2 group in the catalyst structure took part effectively in adsorption rather than photocatalytic removal. A previous study stated that NH_2-functionalized MIL-101(Fe) structure has more light absorptive potentials that allow the transfer of photoelectrons through the ligand to active Fe–O regions [40]. So, the expectation is that the NH_2-functional MIL-101(Fe) catalyst must be more effective in the photocatalytic degradation of imidacloprid. However, similar results were not obtained in this study. The reason of these results can be explained as the electrons on NH_2 were occupied with IMC^+ structure by electrostatic interaction that caused the weakening of the expected photoelectron transfer in the NH_2-MIL (Fe) structure at acidic pH values. So, the photocatalytic efficiency of NH_2-MIL-101(Fe) was obtained the lower percent than MIL-101 (Fe). For example, in case of MIL-101(Fe), after 10% adsorption of IMC, the photocatalytic degradation of IMC was observed as 97% in the end of 15 min. But after adsorption process (removal value of 53%) the photocatalytic efficiency of the NH_2-MIL-101(Fe) reached to only 89% in the end of 15 min.

Photocatalytic activities of amine-functionalized MOFs have also been obtained as low levels in some studies. For example, Fisher 2017 reported that low catalytic effect of a MOF HKUST-1-NH_2 in the Knoevenagel condensation of benzaldehyde and malononitrile, due to the electronic and steric effect of its amino moieties [41]. Also Noh and co workers have investigated carbondioxide cycloaddition reaction by using functionalized UiO-66 MOF with different functional group (NH_2, Br, Cl etc.). In the result of this work, non functionalized UiO-66 MOF has showed the best conversion in the carbon dioxide cycloaddition reaction at the low temperature condition [42].

Three-dimensional (3D) response surfaces

After determining that the catalyst/UV/H_2O_2 system was the most effective, the effects of catalyst amount, IMC concentration, H_2O_2 amount, pH and time on IMC removal were investigated using the response surface method and central composite design and obtained results were given in Table 2. The interactive effect of MIL-101(Fe) amount and the concentration of IMC on removal % at constant H_2O_2 dosage (110 µL), 30 min of treatment time and pH 5.0 is shown in Fig. 10a. When the IMC solution concentration was kept at 40 mg/L, increasing the amount of MIL-101(Fe) catalyst increased the percentage of removal. Conversely, when the concentration was kept at 80 mg/L, the change in the amount of catalyst remained ineffective. Figure 10b presents the interactive effect of IMC concentration and amount of H_2O_2 at constant 0.15 g/L of MIL-101(Fe), pH 5.0 and 30 min of treatment time. The increase of the added amount of H_2O_2 to the system increases the removal efficiency of catalyst. For example, when 75 µL and 150 µL H_2O_2 were added, 87% and 100% removal was achieved, respectively. The effect of pH, the most effective variable, is given in Fig. 10c. Removal of the IMC increases with the pH value of the solution at acidic areas. The increase in photocatalytic processing time is again seen in Fig. 10d as an effective variable in IMC removal.

The effects of variables on the IMC removal was also performed with NH_2-MIL-101(Fe) catalyst containing the amine group and given in Fig. 11. Decrease in IMC removal was observed as the solution pH value increased towards the basic area (Fig. 11a). When the amount of catalyst was increased from 0.12 to 0.20 g/L, the IMC removal increased from 79 to 96% at pH 5.0. In case of using NH_2-MIL-101(Fe) catalyst, the effect of pH similarly provides more efficient removal of IMC in acidic areas.

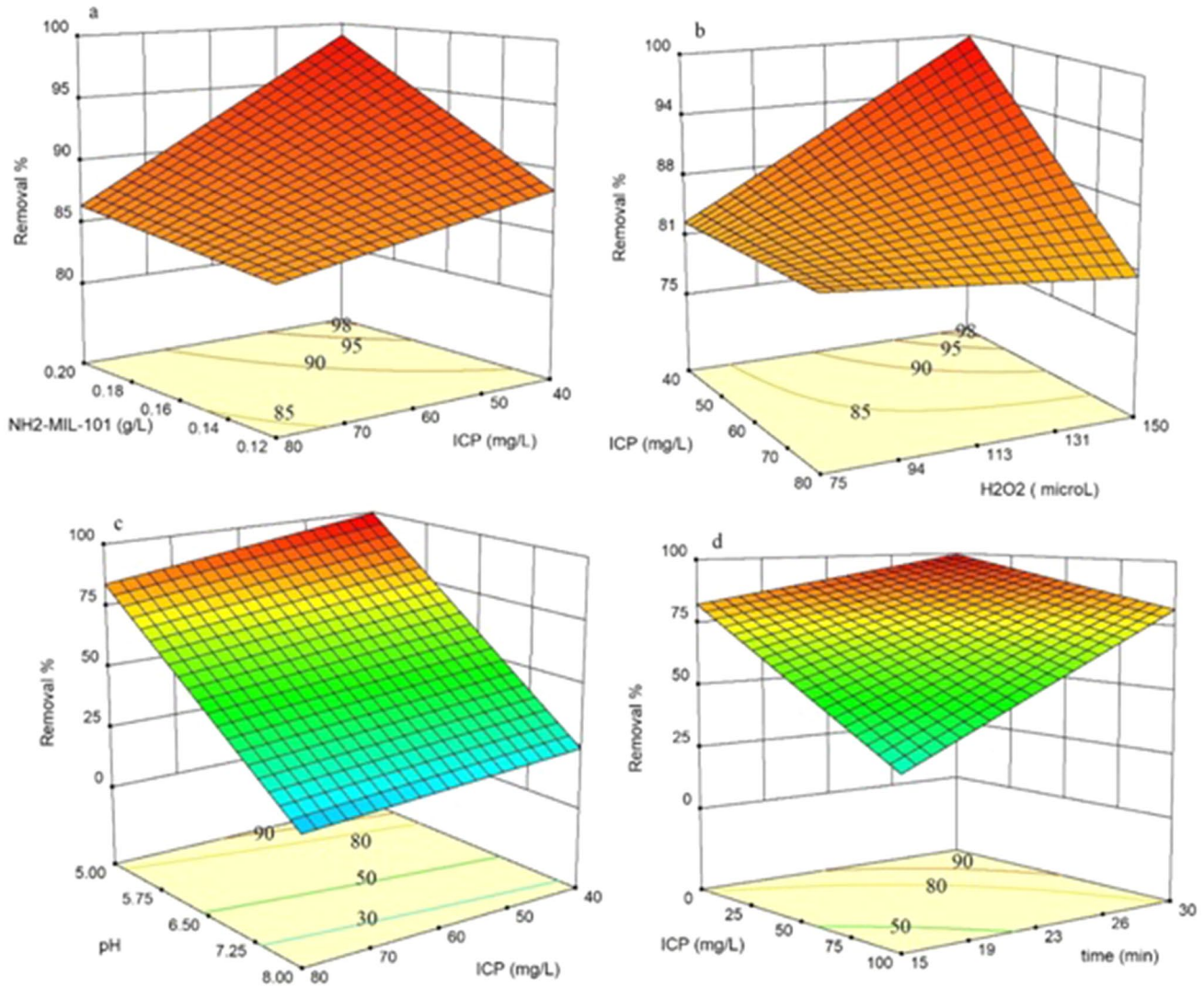

Fig. 10 The interactive effect of **a** MIL-101(Fe) amount and IMC concentration (110 µL of H_2O_2, pH 5.0, 30 min) **b** IMC concentration and H_2O_2 amount (0.15 g/L of MIL-101(Fe), pH 5.0, 30 min) **c** pH and IMC concentration (0.15 g/L of MIL-101(Fe), 142 µL of H_2O_2, 30 min), and **d** IMC concentration and time (0.17 g/L of MIL-101(Fe), 110 µL of H_2O_2, pH 5.0) on removal % of IMC

When 0.20 g/L of catalyst, 80 mg/L of IMC, 150 µL of H_2O_2 ant 30 min of treatment time were applied, IMC removal efficiencies at pH 5, 6.5 and 8, were obtained as 84.5%, 49.5% and 14.5%, respectively (Fig. 11b). Figure 11c shows also that the increase in time was an important parameter in IMC removal and increased the efficiency of degradation.

As a result, optimum application conditions were determined as 40 mg/L IMC, 150 µL H_2O_2, pH 5 and 30 min and at these conditions 100% IMC removal was performed for both catalysts.

Reusability of catalysts

Reusability is particularly important in reactions where solid catalysts are used. Therefore, a four-cycle experiment was performed to check the reusability of MIL-101 materials and the results are shown in Fig. 12. Each experiment was carried out under optimum conditions (40 mg/L IMC, 150 µL H_2O_2, pH 5 and 30 min). After the first run of the photocatalytic process, the catalysts were recovered by centrifuged and then washed thoroughly with water and ethanol. The recovered catalysts were dried under vacuum at 70 °C. At

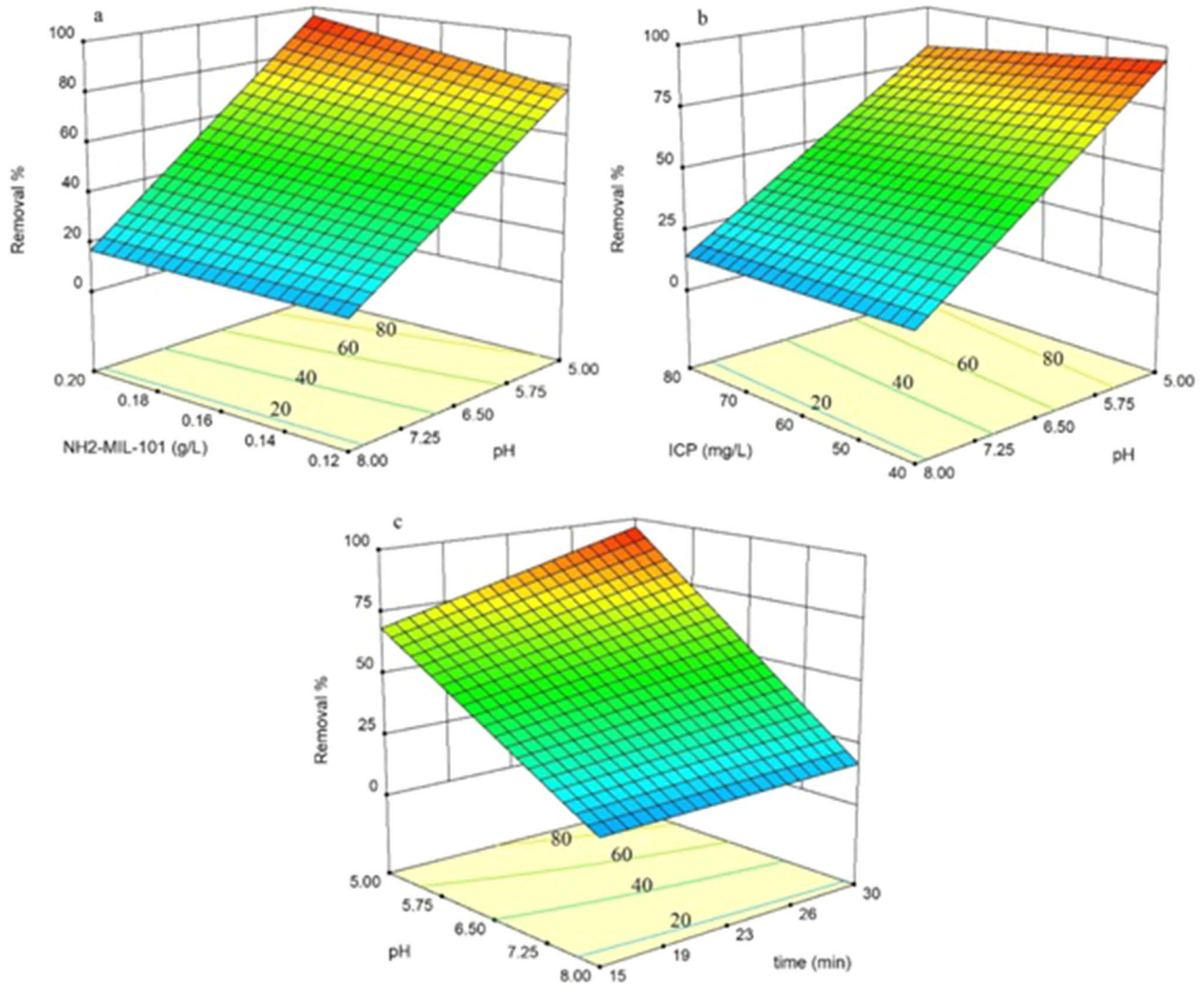

Fig. 11 The interactive effect of **a** NH_2-MIL-101(Fe) amount and pH (150 µL of H_2O_2, 30 min, 40 mg/L of IMC) **b** IMC concentration and pH (0.20 g/L of NH_2-MIL-101(Fe), 150 µL of H_2O_2, 30 min), and **c** pH and time (0.20 g/L of NH_2-MIL-101(Fe), 150 µL of H_2O_2, 40 mg/L of IMC) on removal % of IMC

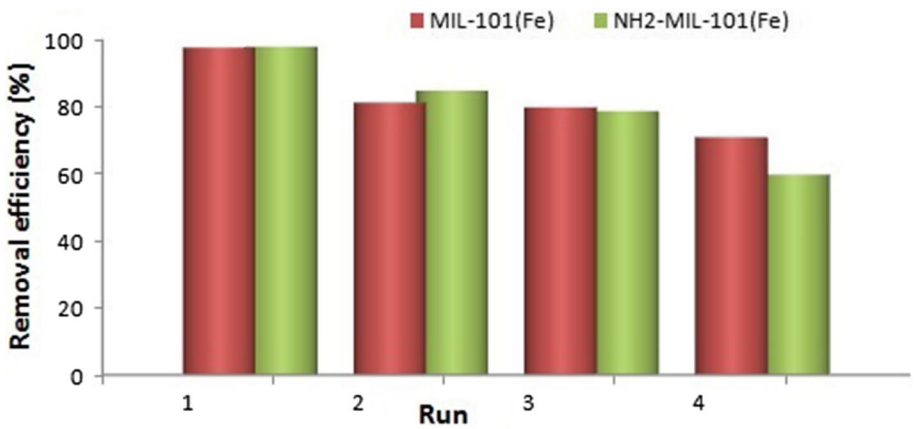

Fig. 12 Reusability of MIL-101(Fe) materials for IMC degradation

the end of 4 runs, the removal efficiencies of MIL-101 (Fe) and NH_2-MIL-101(Fe) catalysts decreased from 100 to 71% and 60%, respectively. This decreasing may be caused by the occupation of active regions with impurities. However, it can be said that the catalysts are reusable in the photocatalytic degradation of the IMC.

Conclusion

The iron-based metal organic framework (MOF) materials MIL-101(Fe) and amine-functionalized NH_2-MIL-101(Fe) were synthesized and characterized in a detail. These MOF materials were used as catalyst for the combined process of adsorption and photodegradation of IMC. The response surface methodology was applied in designing the removal experiments and ANOVA results showed the 2-factor interactions (2FI) model fitted.

Multiple regression modeling of both catalyst showed that the increasing amount of catalysts, H_2O_2 and time have a positive effect, but pH which the most effective variable and concentration of IMC have also a negative effects on the photocatalytic removal of IMC. Also, while the catalyst/UV/H_2O_2 system was significantly effective on the photocatalytic removal of IMC but the NH_2 group in the reduced the removal activity of the catalyst.

On the other hand, the adsorption power of the NH_2-MIL-101(Fe) catalyst was significantly higher than that of MIL-101(Fe) and was found to be much more effective due to electrostatic interaction at acidic pH values. After the one-hour adsorption–desorption period, photocatalytic process was applied and 100% IMC removal was performed by using MIL-101(Fe) and NH_2-MIL-101(Fe) as catalysts at optimum application conditions (40 mg/L IMC, 150 µL H_2O_2, pH 5 and 30 min). As for reusability, the MIL-101 materials showed good catalytic performance in sequential experiments.

Funding This work was supported by the research fund of Mersin University in Turkey under grant [2017-1-AP4-2224].

References

1. G. Liu, L. Li, D. Xu, X. Huang, X. Xu et al., Carbohydr. Polym. **175**, 584–591 (2017)
2. Y. Pi, X. Li, Q. Xia, J. Wu et al., Chem. Eng. J. **337**, 351–371 (2018)
3. M. Zhang, W. Zhou, T. Phan, K.A. Forrest et al., Angew. Chem. Int. Ed. **56**, 11426–11430 (2017)
4. S. Beatriz, T. Carlos, C. Joaquín, S. Claudia, Sep. Purif. Technol. **111**, 72–81 (2013)
5. P. Karthik, A. Pandikumar, M. Preeyanghaa, M. Kowsalya, B. Neppolian, Microchim. Acta **184**, 2265–2273 (2017)
6. J. Gordon, H. Kazemian, S. Rohani, Mater. Sci. Eng. C **47**, 172–179 (2015)
7. Q. Xie, Y. Li, Z. Lv, H. Zhou, X. Yang, J. Chen, H. Guo, Nat. Sci. Rep. **7**, 3316 (2017)
8. K. Leus, Y.Y. Liu, P.V.D. Voort, Catal. Rev. Sci. Eng. **56**, 1–56 (2014)
9. C. Gao, S. Chen, X. Quan, H. Yu, Y. Zhang, J. Catal. **356**, 125–132 (2017)
10. P. Serra-Crespo, E.V. Ramos-Fernandez, J. Gascon, F. Kapteijn, Chem. Mater. **23**, 2565–2572 (2011)
11. T. Hu, Q. Jia, S. He, S. Shan, H. Su, Y. Zhi, L. He, J. Alloys Compd. **727**, 114–122 (2017)
12. D.-X. Xue, Q. Wang, J. Bai, Coord. Chem. Rev. (2017) https://doi.org/10.1016/j.ccr.2017.10.026
13. A.J. Emerson, A. Chahine, S.R. Batten, D.R. Turner, Coord. Chem. Rev. **365**, 1–22 (2018)
14. P. Karthik, R. Vinoth, P. Zhang, W. Choi, E. Balaraman, B. Neppolian, ACS Appl. Energy Mater. (2018) https://doi.org/10.1021/acsaem.7b00245
15. R. Ahmad, N.M. Salem, H. Estaitieh, Chemosphere **78**, 667–671 (2010)
16. S. Samsidar, S.M. Siddiquee, Shaarani, Trends Food Sci. Technol. **71**, 188–201 (2018)
17. M.A. Radwan, M.S. Mohamed, Ecotoxcol. Environ. Saf. **95**, 91–97 (2013)
18. S. Baskaran, R.S. Kookana, R. Naidu, J. Chrom A. **787**, 271–275 (1997)
19. S. Malato, J. Caceres, A. Aguera, M. Mezcua, D. Hernando, J. Vial, A.R. Fernández-Alba Environ. Sci. Tech. **35**, 4359–4366 (2001)
20. K.A. Sumon, A.K. Ritika, E.T.H.M. Peeters, H. Rashid, R.H. Bosma, M.S. Rahman, M.K. Fatema, P.J. Van den Brink, Environ. Pollut. **236**, 432–441 (2018)
21. H.R. Ghalebi, S. Aber, A. Karimi, J. Mol. Catal. A Chem. **415**, 96–103 (2016)
22. S.G. Zhang, L.N. Li, S.G. Zhao, Z.H. Sun, J.H. Luo, Inorg. Chem. **54**, 8375–8379 (2015)
23. P.L. Feng, I.V.J.J. Perry, S. Nikodemski, B.W. Jacobs, S.T. Meek, M.D. Allendorf, J. Am. Chem. Soc. **132**, 15487–15489 (2010)
24. M.A. Bezerra, R.E. Santelli, E.P. Oliveira, L.S. Villar, L.A. Escaleira, Talanta **76**, 965–977 (2008)
25. R. Bruns, I. Scarmino, B. de, *Baros neto, statistical design—chemometrics*, 1st edn. (Elsevier, Amsterdam, 2008), p. 422
26. A.D.S. Barbosa, J.D. Fernandes, A.F. Peixoto, C. Freire, B. de Castro, C.M. Granadeiro, S.S. Balula, L. Cunha-Silva, Polyhedron **127**, 464–470 (2017)
27. M. Saikia, V. Kaichev, L. Saikia, RSC Adv. **6**, 106856–106855 (2016)
28. D. Jiang, L.L. Keenan, A.D. Burrows, K.J. Edler, Chem. Commun. **48**, 12053–12055 (2012)
29. S.S. Bayazit, S.T. Danalioglu, M. Abdel Salam, O. Kerkez, Environ. Sci. Pollut. Res. Int. **24**, 25452–25461 (2017)
30. D.K. Panchariya, R.K. Rai, S.K. Singh, E.A. Kumar, Mater. Today Proc. **4**, 388–394 (2017)
31. Y. Liu, P. Gao, C. Huang, Y. Li, Sci. China Chem. **58**, 1553–1560 (2015)
32. Y. Zang, J.S. Zhang, Y. Zhong, W. Zhu, Catal. Sci. Technol. **3**, 20–44 (2013)
33. C.P. Cabello, G. Berlier, G. Magnacca, P. Rumori, G.T. Palomino, Cryst. Eng. Comm. **17**, 430–437 (2015)
34. E.P. Barrett, L.G. Joyner, P.P. Halenda, J. Am. Chem. Soc. **73**, 373–380 (1951)
35. S. Brunauer, P.H. Emmett, E. Teller, J. Am. Chem. Soc. **60**, 309–319 (1938)
36. M. Almáši, V. Zeleňáka, P. Palotaia, E. Beňováa, A. Zeleňáková, Inorg. Chem. Comm. **93**, 115–120 (2018)

37. W. Xiong, Z. Zeng, X. Li, G. Zeng, R. Xiao, Z. Yang, Y. Zhou, C. Zhang, M. Cheng, L. Hu, C. Zhou, L. Qin, R. Xu, Y. Zhang, Chemosphere **210**, 1061–1069 (2018)
38. K. Chamberlain, A.A. Evans, R.H. Bromilow, Pestic. Sci. **47**, 265–271 (1996)
39. M.J. Katz, S.Y. Moon, J.E. Mondloch, M.H. Beyzavi, C.J. Stephenson, J.T. Hupp, O.K. Farha, Chem. Sci. **6**, 2286–2291 (2015)
40. C.G. Silva, J.L. Faria, J. Photochem. Photobiol. A **155**, 133–143 (2003)
41. M. Fischer, Der Technischen Fakultät der Friedrich-Alexander-Universität Erlangen-Nürnberg. PhD Thesis (2017)
42. J. Noh, Y. Kim, H. Park, J. Lee, M. Yoon, M.H. Park, Y. Kim, M. Kim, J. Ind. Eng. Chem. **64**, 478–483 (2018)